International Journal of Applied Earth Observations and Geoinformation 117 (2023) 103194

Contents lists available at ScienceDirect

International Journal of Applied Earth Observations and Geoinformation

journal homepage: www.elsevier.com/locate/jag

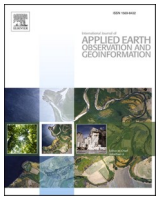

Integration of multi-sensor MTInSAR and ground-based geomatic data for the analysis of non-linear displacements affecting the urban area of Chieuti, Italy

Alberico Sonnessa [a,*], Annamaria di Lernia [a], Davide Oscar Nitti [b], Raffaele Nutricato [b], Eufemia Tarantino [a], Federica Cotecchia [a]

[a] Department of Civil, Environmental, Land, Construction and Chemistry (DICATECh), Polytechnic University of Bari, 70125 Bari, Italy
[b] Geophysical Applications Processing s.r.l., c/o Physics Department of Polytechnic University of Bari, 70126 Bari, Italy

ARTICLE INFO

Keywords:
Non-linear instability phenomena
Multi-sensor MTInSAR
COSMO-SkyMed
Sentinel-1
Non-linear displacement trend reliability assessment
Geomatic monitoring techniques

ABSTRACT

Slow instability phenomena can turn into rapid events, showing sudden accelerations and potentially developing in a threat for structures and people. In such scenarios, an in-depth understanding of the spatial and temporal evolution of the ground surface displacement field becomes essential for preventing potential catastrophes. In this work, Multi-Temporal Interferometry SAR (MTInSAR) technique based on COSMO-SkyMed and Sentinel-1 SAR acquisitions and ground measurements have been used to study an ongoing instability occurrence, affecting the urban area of Chieuti, a town located in the Southern Italy. Archives of C and X-band SAR data and geomatic monitoring observations spanning seven, five and one year, respectively, have been analyzed exploiting the complementary characteristics of these datasets. This enabled the accurate spatial-temporal characterization of the ground displacement field in the study area, the identification of sectors evidencing instability problems and a comprehensive reliability assessment of the detected displacements trends, characterized by strong non-linearities. Moreover, the multi-geometry DInSAR analysis allowed to evaluate the horizontal and vertical components of the detected motion, confirming the nature of the instability process, related to a deep landslide mechanism affecting the western slope of the town.

1. Introduction

Slow ground instability phenomena involving the built environments may impact the safety of structures and people (Sonnessa et al., 2020), since the decay of the structures' integrity can lead to fragile collapse (Hungr et al., 2014). Furthermore, slow displacements resulting from the progression of failure underground (Chandler et al., 1975; Potts et al., 1997) can determine the transition from slow to rapid and catastrophic events, as made evident by the Vajont disaster (Alonso et al., 2010). Therefore, the prevention of damage and collapse of structures and infrastructures (Achu et al., 2021; Morgese et al., 2020; Nibigira et al., 2018) benefits from the thorough knowledge of the spatial and temporal evolution of the ground surface displacement fields, even for low motion rates (Cotecchia et al., 2020; Dai et al., 2002; Esposito et al., 2021).

The geomatic monitoring of structures and ground surface is often carried out by integrating different methodologies (Furst et al., 2021; Karila et al., 2013), such as automated total stations (Artese & Perrelli, 2018; Crespi et al., 2012), high-precision geometric levelling (de Luna et al., 2017; Hsu et al., 2018), Synthetic Aperture Radar (SAR) (Mazzanti et al., 2015; Milillo et al., 2016; Scifoni et al., 2016) or Global Navigation Satellite Systems (Del Soldato et al., 2018; Sonnessa & Tarantino, 2021).

In the last thirty years, the increasing number of Earth observation satellite missions has made available a huge amount of data, providing a consolidated tool for Civil Protection institutions in addressing landslide risk (Raspini et al., 2017), due to the possibility of investigating ground shifts of large areas over years the with a progressively smaller revisit time, equal to few days for the most recent satellite sensors. In this field, the European Space Agency (ESA) plays a crucial role (Raspini et al., 2018) through the Copernicus Programme including Sentinel-1 (S1) satellites and contributing missions, such as COSMO-SkyMed (CSK). S1 consists of two quasi-polar-orbiting satellites, mounting a SAR sensor that operates in C-band. CSK, exploiting the X-band, comprises four

* Corresponding author at: DICATECh, Polytechnic University of Bari, Via Orabona 4, 70125 Bari, Italy.
E-mail address: alberico.sonnessa@poliba.it (A. Sonnessa).

https://doi.org/10.1016/j.jag.2023.103194
Received 10 August 2022; Received in revised form 10 January 2023; Accepted 11 January 2023

Fig. 1. a) Chieuti, located at the borders between Molise and Apulia Italian regions; b) the hillslope affected by slope movements (in the white square).

quasi-polar-orbiting satellites.

Data acquired by means of space-borne SAR sensors and processed through MTInSAR techniques represent a powerful tool to support the analysis of natural hazards, such as ground deformation phenomena involving infrastructures and buildings (Calò et al., 2014; Uemoto et al., 2019). The capability of covering wide areas with a high-frequency temporal sampling allows to investigate diffuse instability through Persistent Scatterer Interferometry (PSI) (Crosetto et al., 2016; Ferretti et al., 2001), which provide information about displacements and displacement rates along the line-of-sight (LoS) of scatterers distributed in the target area. However, uncertainties may affect the assessment of the displacement patterns when the investigated phenomenon is characterized by a strong non-linear evolution (Shi et al., 2020).

This paper reports the results of a research work within which multi-sensor MTInSAR data and ground-based techniques were combined to evaluate the development of the displacements generated by the low progression of a complex instability process (Cruden and Varnes, 1996), affecting the urban area of Chieuti, in Southern Italy, characterized by non-linear stages of the displacement–time evolution. The area is under the attention of the Government Commissioner for the environmental risk of the Apulia region, which oversees the implementation of proper risk mitigation strategies and funded the research work, aimed at the analysis and interpretation of a relatively large stack of X and C-band SAR data, acquired by means of CSK and S1 satellites respectively, over a timespan of seven years (2015–2022).

The analysis of the multi-sensor MTInSAR data, performed through the SPINUA algorithm developed by GAP, a spinoff company of the Polytechnic University of Bari, has been integrated by measurements obtained through a high-precision geometric levelling, designed on the basis of the MTInSAR analysis findings, in order to investigate the outcropping effects of the instability phenomenon within the western slope of the urban centre, recognised to be subsiding since 1800.

The study provided a comprehensive spatial and temporal characterisation of the displacement field at the top of the slope, allowing for the recognition of the instability area as the active retrogressive rear scarp of a landslide. Furthermore, the obtained results shed novel light on the reliability and consistency of the MTInSAR techniques in proper detecting non-linear ground displacement patterns. Once examined considering the framework of geomorphological and geo-mechanical characteristics of slope failures, the achieved outcomes have supported the hypothesis that the underground failure is connected to the current activity of very large soil volumes downslope.

2. The town of Chieuti

Chieuti is a small town located close to the northern border of Apulia, in the south of Italy (Fig. 1**a**). The old town, perched on a hilltop at 221 m a.s.l, is characterized by the presence of masonry buildings and narrow streets. The western side of the site is bounded by the Taverna canal to the north, and the Fico stream valley to the west (Fig. 1**b**). The hillslope is formed of a foredeep marine succession, where stiff clays (Montesecco clay formations, Pliocene) underlie a layer of marine regression sands and sandy silts (Serracapriola sand formation, Pleistocene). The historical centre is built above a top-hill thinner continental layer, made of fine soil matric including coarser grains, which overlies the marine deposits.

Evidence of instabilities involving the old town along the top of the western slope has been logged since the first decades of 1800, as reported by municipal archive documents referring to collapse and demolition of buildings, located in the north-western sector bordered by Largo Quattro Novembre, Via dei Martiri di Via Fani and part of Via Vitalia (Fig. 1**b** and Fig. 2**a**). Buildings located westward the red dash-dotted line (Fig. 2**a**) have suffered from the cumulation of mainly downward displacements, caused by ground instability processes never thoroughly characterized.

In the last 60 years, several mitigation interventions, encompassing retaining structures and storm water management works, have been set in place at the western edge of the urban centre to minimize the damages, with limited success. The last intervention, built between 2004 and 2006 (yellow line in Fig. 2**a**), consists of a concrete counterfort retaining wall (Fig. 2**b**) on pile foundations (12 m long piles of 80 cm diameter arranged in quincunx) connected to the pre-existing counterfort wall

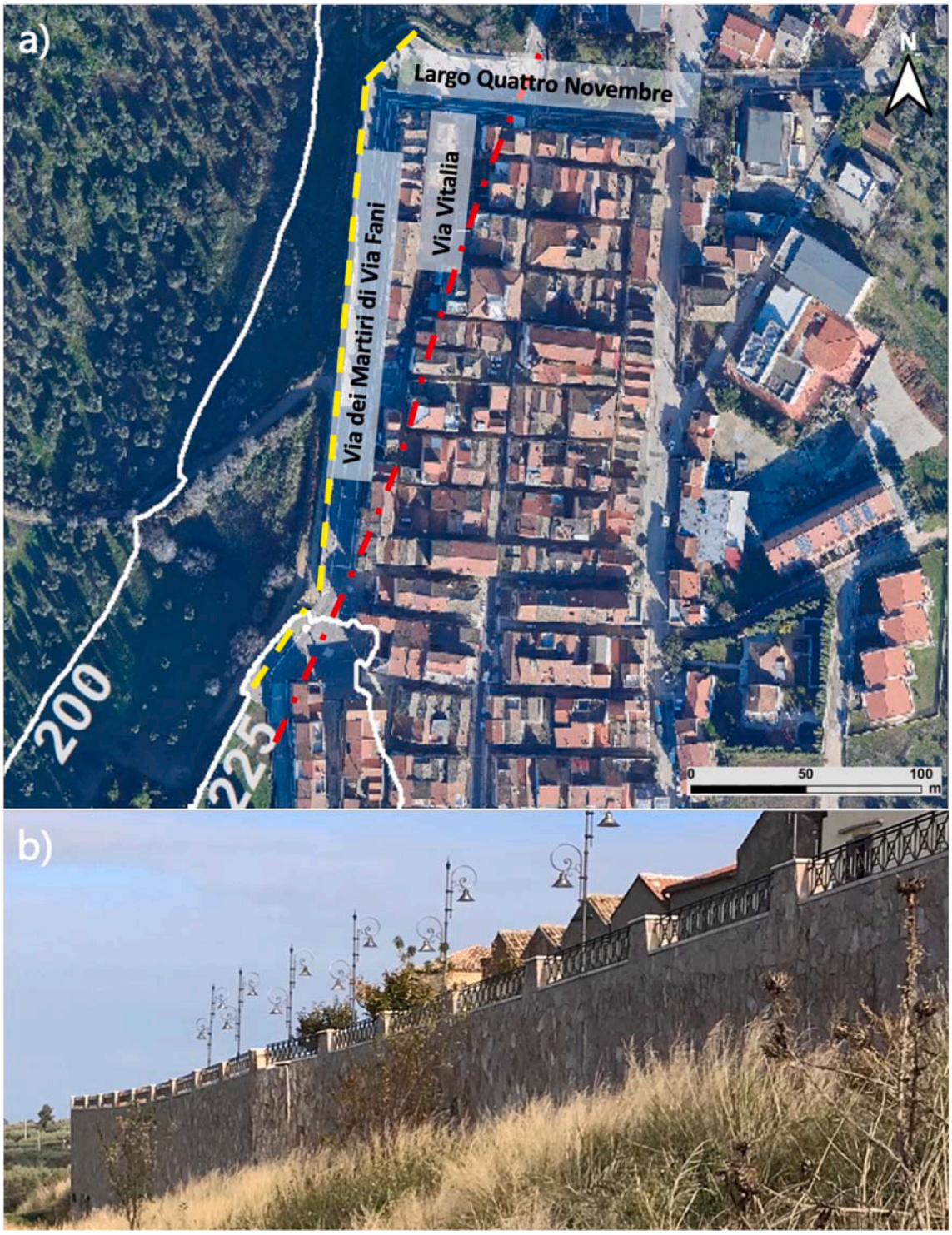

Fig. 2. a) Sector of the old town involved in the instability phenomenon and b) view of the retaining structure located along Via dei Martiri di Via Fani.

founded on shallow footings (dated 1987–1989). These engineering operas are currently damaged, as shown in **4.1**.

3. Employed methodologies

In the study, MTInSAR techniques provided an insight into the magnitude and the spatial–temporal evolution of the ground displacement field suffered by the built area, while high-precision geometric levelling complemented the analysis validating the deformation patterns.

3.1. High-precision geometric levelling

High-precision geometric levelling is a well-established geomatic technique, widely used for monitoring ground movements and controlling structures (Bitelli et al., 2018). The methodology allows the measuring of height differences through automatic levels and invar rods, on benchmarks built on purpose in the monitored areas, with accuracy up to few tenth of millimeters (Vaníček et al., 2001).

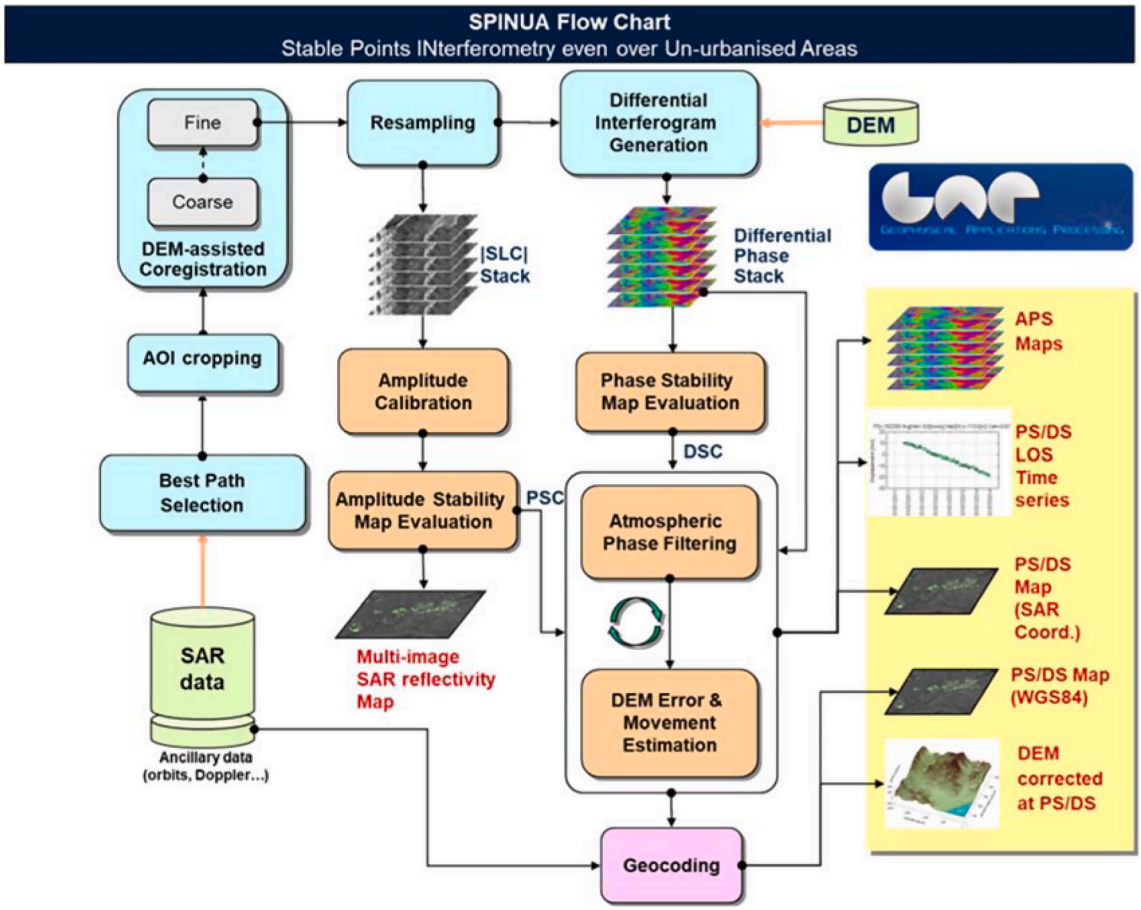

Fig. 3. SPINUA flow chart modified from (Bovenga et al., 2005).

Table 1
Main characteristics of the exploited SAR datasets.

Satellite	Acquisition mode	Spatial resolution (AzimuthxRange)	Wavelength (λ)	Pass direction	Best temporal resolution on the area	Timespan	Number of images	Incidence angle	Heading angle
CSK	Stripmap/Himage	3mx3m	3.1 cm	Ascending	16 days	Jan 2015-Dec 2020	58	32,0°	169,2°
				Descending		Feb 2016-Dec 2020	71	31,0°	10,9°
S1	Interferometric wide-swath	20mx5m	5.6 cm	Ascending	6 days (12 days after December 2021)	Apr 2015-May 2022	367	42,1°	170,4°
				Descending		Apr 2015-May 2022	361	41,2°	9,7°

3.2. MTInSAR approach and the SPINUA algorithm

MTInSAR approach makes use of the coherent image principle of SAR, whereby the intensity and the phase of the received signal is recorded. SAR sensors send out a pulse of electromagnetic waves and measure amplitude and phase of the signal reflected or scattered back from the target material. By exploiting the phase differences among the backscattered signals of SAR acquisitions displaced in time and received from slightly different positions, MTInSAR techniques allow to measure ground surface displacements with sub-centimetric or even millimetric precision. The methodology is based on the identification of coherent targets, i.e. Persistent Scatterers (PS), associated with a single pixel, and Distributed Scatterers (DS), related with a group of statistically homogeneous pixels, whose reflectivity is sufficiently independent from both temporal and geometric baselines, and with high phase stability. MTInSAR technique limitations are mainly related to the lack of PS in vegetated areas, the need of a reference point for the retrieved displacements, the detection of the displacements along the LoS and a very low sensitivity to the North-South component, due to the quasi-polar orbits of the current satellite missions.

In this work, the MTInSAR SPINUA algorithm (Bovenga et al., 2005), whose processing flow is illustrated in Fig. 3, has been employed. The algorithm has been successfully applied to detect the evidences of infrastructure instabilities, and validated by comparison with in-situ measurements (Bovenga et al., 2013; Radicioni et al., 2012) and cross-comparisons with other MTInSAR techniques (Reale et al., 2011; Wasowski & Bovenga, 2015).

The stack of focused images in input is co-registered using the approach presented in (Nitti et al., 2011); a further alignment step is applied to S1 data, as highlighted in (Prats-Iraola et al., 2012). The InSAR processing allow to generate the stack of differential interferograms. Image calibration enables the detection of both candidate PS

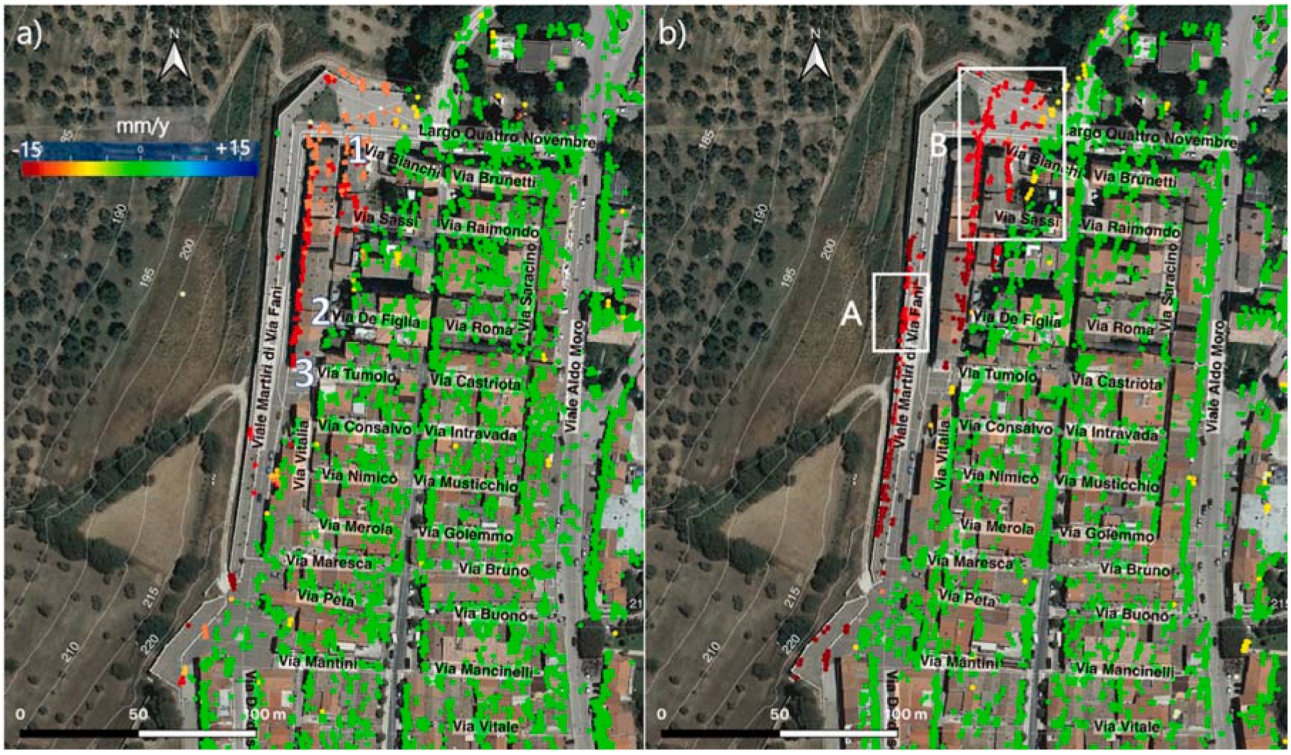

Fig. 4. a) Ascending and b) descending mean velocity maps resulting from the processing of the CSK datasets between January 2015 and December 2020, with a) the location of damages (1, 2 and 3) indicated in Fig. 7 and b) clusters A and B within white squares evidencing differential displacements.

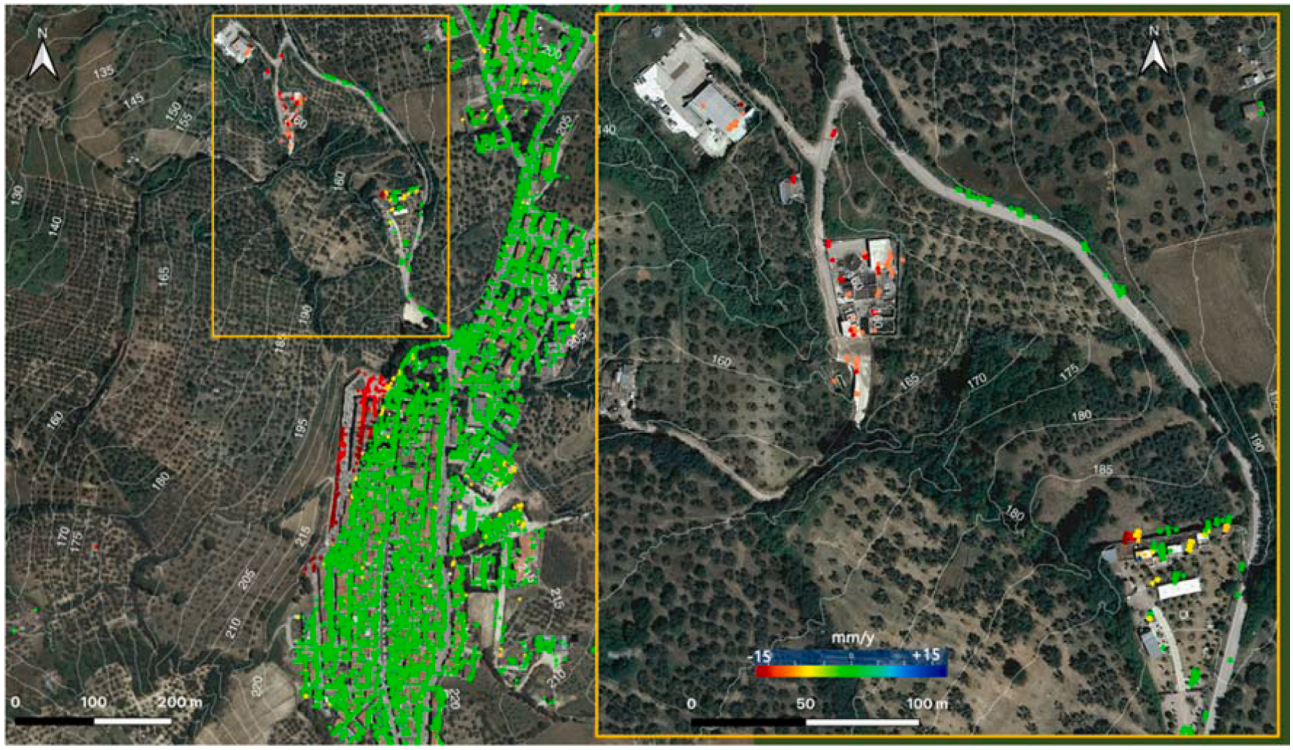

Fig. 5. Mean CSK velocity map (descending orbit) of the study area, with a magnification of the purification plant in the orange square. (For interpretation of the references to colour in this figure legend, the reader is referred to the web version of this article.)

Fig. 6. Damages on the retaining wall (indicated by the red arrow) and the adjacent sidewalk. The dashed line borders a) the sector location of a marked subsidence compared to the surrounding area, displayed in b) and c). (For interpretation of the references to colour in this figure legend, the reader is referred to the web version of this article.)

(PSC) and DS (DSC) (Bovenga et al., 2005; Even & Schulz, 2018; Ferretti et al., 2001), which phase values are used to remove atmospheric/orbital artifacts from the input differential phase, with a robust kriging-based interpolation (Even and Schulz, 2018). The resulting stack of rephased differential interferograms is then analyzed inter-image to improve the PS/DS spatial density and perform a joint estimation of their height and displacement time series, whose reliability is measured through the temporal coherence.

The following contributions are also estimated and corrected for minimizing inconsistencies in geolocation: atmospheric signal delay, azimuth bistatic residual correction (Schubert et al., 2015), and azimuth/range sub-pixel position estimation of point scatterers.

With reference to the height estimation of PS/DS of the analyzed datasets, S1 shows a much lower sensitivity to topography than CSK, since the S1 orbital tube was mainly designed to facilitate DInSAR approaches in displacement mapping, where short perpendicular baselines are more favorable (Barat et al., 2015). This limitation results in a lower vertical geolocation accuracy of the PS detected by processing the S1 datasets. Therefore, the absolute height of S1 targets has been corrected by using a high-resolution 0.5 × 0.5 m Light Detection And Ranging (LiDAR) point cloud available over the scene (Hu et al., 2019a).

4. Characterization of the ground surface displacement field through MTInSAR analysis

The MTInSAR analysis was based on four interferometric datasets, listed in Table 1. An extensive assessment of the trends detected using the different sensors and the corresponding possible ambiguities/limitations in the study context has been performed. Since the analysis was intended to exploit the best available spatial resolution, the interpretation of the displacement field across the built environment relied on the examination of PS. Moreover, the absence of deformations of the masonry structures (small rigid buildings) has been assumed as hypothesis.

Thanks to the high variability of the CSK orbital tube (over 1 km), enabling a precise estimation of the scatterer height (<1 m), and the high spatial resolution, such sensors provided the generation of accurately geocoded PS, allowing a precise identification of unstable areas, which cannot be reached by the S1 sensors, characterized by a relatively poor spatial resolution (Table 1). Conversely, the reduced revisit time of S1 satellites ensured a tight monitoring of the surveyed zone, useful for the detection of relatively rapid velocity variation in case of non-linear displacements.

4.1. Analysis of the settlement area using CSK data

CSK mean velocity maps retrieved along the ascending and descending orbits (Fig. 4) were estimated along the satellite LoS over the period Jan. 2015–Dec. 2020. Negative values indicate motions away from the sensor. The maps highlight the spatial features of the ground surface displacement field, which involves the top of the slope, confirming that part of the settling area (about 9000 m^2) is bordered by Via dei Martiri di Via Fani, Largo Quattro Novembre and the north part of Via Vitalia, and structures around the purification plant located in the north-western sector of the slope (Fig. 5). This finding proves that the

Fig. 7. Damages caused by differential displacements between the stable (indicated with green arrows) and unstable area (highlighted with red arrows) on 1) Via Bianchi, 2) via De Figlia and 3) Via Tumolo. (For interpretation of the references to colour in this figure legend, the reader is referred to the web version of this article.)

displacements affecting the old urban center are connected to an instability mechanism involving at least part of the western slope.

Negative displacement rates, representing downward movements, range from millimeter to centimeter per year, with the lowest values equal to −12 mm/year along the ascending orbit and −16 mm/year on the descending track. The favorable orientation of the structures, placed in alignments nearly perpendicular to the LoS, and the expected direction of motion, which is assumed to follow the steepest path (i.e. west–northwest), made the observations along the descending track (Fig. 4) particularly suitable to detect most part of the displacements. A detailed analysis of the map in Fig. 4**b** suggests that clusters A and B are lowering more slowly with respect to the neighboring areas. Focusing on Via dei Martiri di Via Fani, the cluster A (average velocity of −9 mm/year) moves away from the sensor more slowly than the surrounding portions of the retaining wall and footpath infrastructure (displacement rates of about −12 mm/year), giving rise to differential displacements whose effects are visible on site, as exemplified by the cracks running through the retaining wall and along the Via dei Martiri di via Fani footpath (Fig. 6) and damages on buildings and road pavements crossing 1) Via Bianchi, 2) via De Figlia and 3) Via Tumolo (3) (Fig. 7), located at the border between the stable area, characterized by almost null displacement rates, and the unstable area, identified by high displacement rates (Fig. 4). Velocities vary from significant values to zero along west-east sections, occurring in a narrow west-to-east distance in the southern part of the subsiding area, and developing across a larger distance in the northern part, characterized by more extended differential movements (e.g. red to yellow to green dots in cluster B). This spatial distribution (Fig. 4) is indicative of a currently active retrogression of underground processes, already significantly developed in the northern portion. Such process match the typical effect of the retrogression of underground progressive failure within the rear scarp, related to the activity of very large soil volumes downslope and classifiable as compound roto-translational (Cruden and Varnes, 1996), which brings about the outcropping of multiple rear scarps, where the more recent one is identified by the red line in Fig. 2.

The temporal evolution of the instability emerges from the analysis of a PS subset (points A-L in Fig. 8), distributed from south to north in the subsiding area, selected by applying the coherence value threshold of 0.7, to provide more reliable results. The related displacement time series (Fig. 9) indicate maximum values ranging from about 30 mm to 70 mm away from the sensor over the period Feb. 2016–Dec. 2020, giving evidence to a peculiar subsidence trend, common to all points.

Almost linear motion patterns are interspersed by short acceleration stages, during which the displacement increments are equal, on average, to about 10 mm (Fig. 9), hence of the same magnitude as the CSK motion ambiguity limit, occurring when the difference between two consecutive measurements exceeds a quarter of the sensor wavelength. This required a further analysis to check whether they are affected by motion ambiguity artifacts.

Fig. 8. High-coherence PS (≥ 0.7) extracted from the CSK displacement map along the descending track. The red dots identify the targets investigated. (background: LiDAR Digital Elevation Model). (For interpretation of the references to colour in this figure legend, the reader is referred to the web version of this article.)

4.2. Evaluation of the non-linear displacement trends through the combined analysis of CSK and S1 datasets

CSK time series are affected by ambiguities when the displacements are greater than 7.8 mm (i.e. $\lambda/4$) in 16 days (Table 1). The availability of SAR sensors working with different wavelengths offers the opportunity to assess the reliability of the trends detected. To this aim, additional PS from S1 measurements along the descending track have been selected using as reference CSK PS (Fig. 8), with the following criteria:

1. temporal coherence ≥ 0.7;
2. planimetric distance from the reference CSK PS ≤ 10 m (half of the S1 range resolution);
3. altimetric distance (dH) from the reference CSK PS $-1.5 \leq dH \leq 1.5$ m;
4. difference in velocity along the LoS $|v\ LoS^{CSK} - v\ LoS^{S1}| \leq 1.5$ mm/year.

The comparison between the two datasets is shown in Fig. 10, where CSK-derived reference time series are superimposed with the

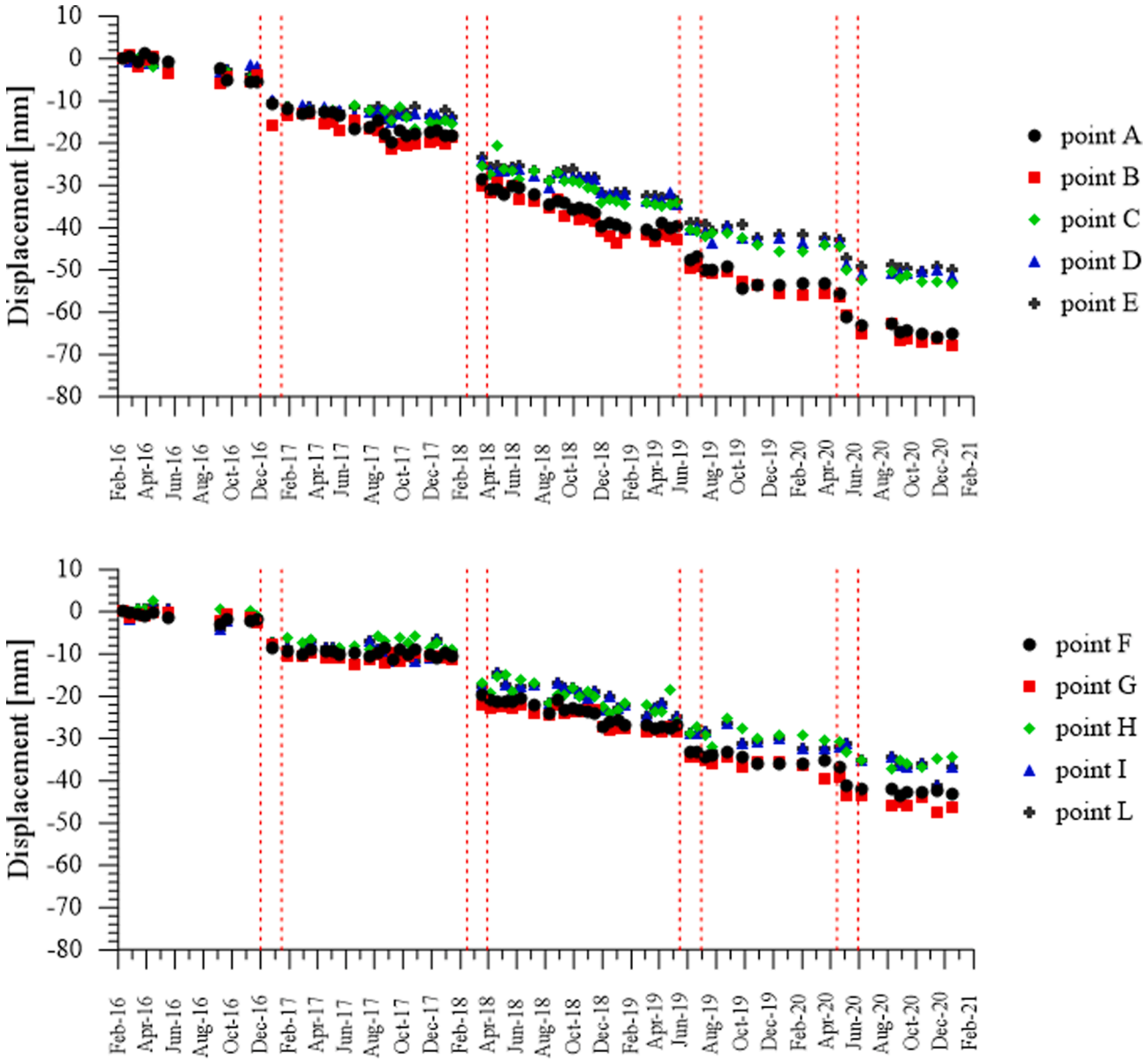

Fig. 9. CSK LoS displacement time series (Feb. 2016–Dec. 2020) of the target A to L. The red-dashed lines indicate the acceleration stages. (For interpretation of the references to colour in this figure legend, the reader is referred to the web version of this article.)

corresponding related to single PS obtained from S1 observations. Levelling measurements acquired from May 2021 to May 2022 are also displayed (green triangles) and will be discussed in section 5. The largest cumulative displacements are measured in the southern sector (scatterers A and B), reaching a maximum of 100 mm, while displacements of about 50–60 mm have been detected in the north part of the old town (scatterers H and I) and at the purification plant (point L). Both datasets confirm the non-linear features of the displacement evolution, but the extended temporal coverage and high temporal resolution of S1 observations enable further consideration on its progress. The acceleration stages, recurring approximately once a year, show a duration of about one month (dashed lines in Fig. 10), while between two steps the velocities are almost constant and relatively low (~7–13 mm/year) over periods of 10 to 16 months.

As S1 time series can tolerate displacements up to 14 mm ($\lambda/4$ according to Table 1) every 6 days, and considering the average magnitudes of the detected steps (10 mm in one month, well below the 14 mm S1 ambiguity limit), the analysis of S1 time series confirms that this trend is not caused by phase unwrapping ambiguity errors due to motion. In addition, the strong advantages in proper tracking non-linear shifts and correcting potential artifacts, derived from the integration of the datasets, are highlighted examining the point G (Fig. 11), for which S1 observations allowed to correct the CSK original trend (green squares), shifted of $\lambda/2$ after March 16, 2020 (red squares).

To rule out connections between the detected steps and modifications in the scattering mechanism, which could introduce phase changes misinterpreted as displacement steps, also amplitude time series have been considered. The effect of a backscattering coefficient (σ_0) alteration can be observed in Fig. 12, showing the plot of a target relative to a building interested by reroofing works a) and the associated displacement time series b) evidencing a fictious shift of about 10 mm in September 2015. Conversely, the CSK backscattering coefficient of the analyzed PS (Fig. 13) exhibit no significant variations, thus confirming that the steps identified cannot be ascribed to artifacts.

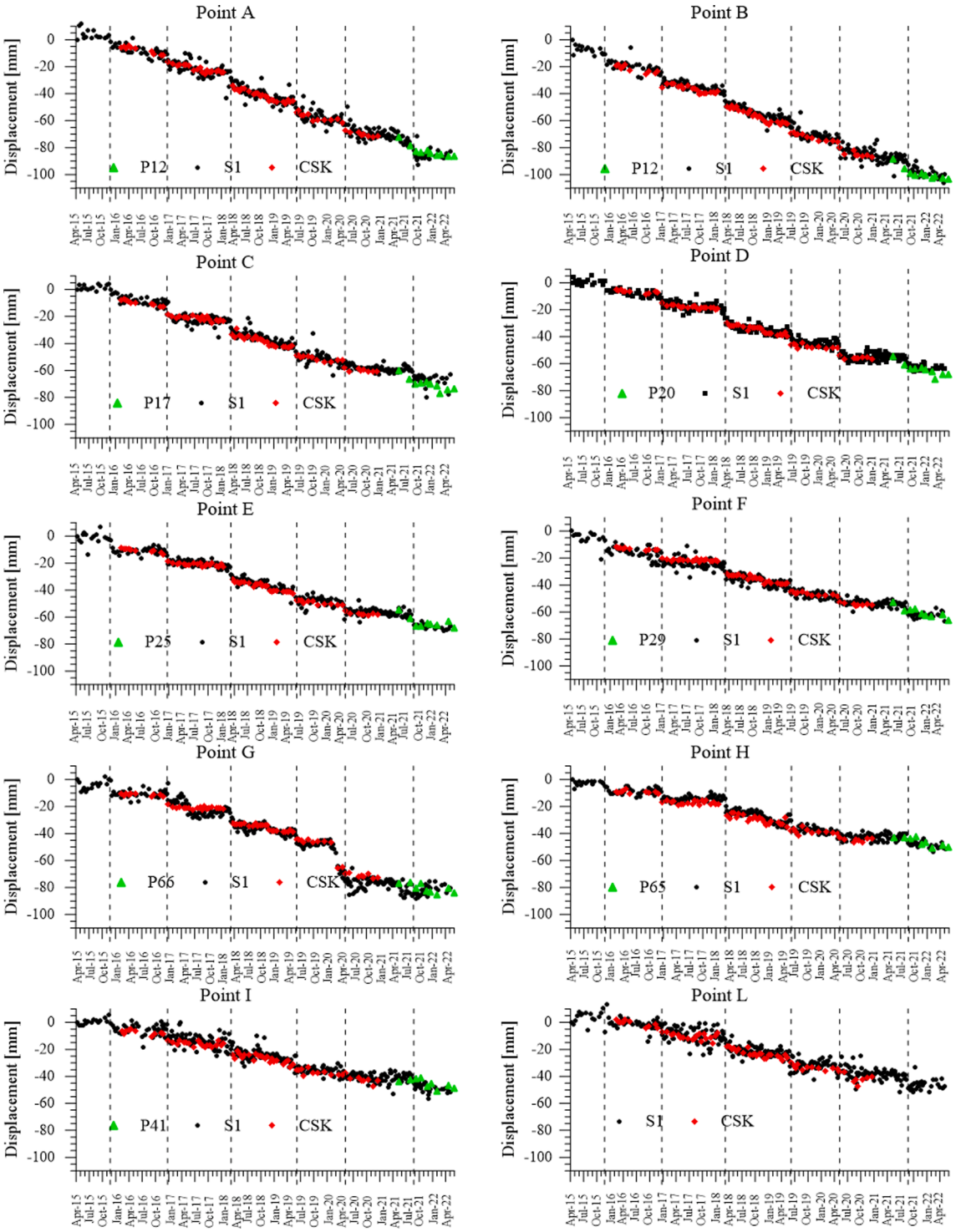

Fig. 10. LoS displacement time series relating to the CSK targets A-L (red dots) compared to those extracted from the S1 descending displacement map (black dots), covering the period Apr.2015–May 2022. Dashed lines indicate the displacement acceleration stages. Green triangles represent the levelling measurements referring to benchmarks available around the PS. (For interpretation of the references to colour in this figure legend, the reader is referred to the web version of this article.)

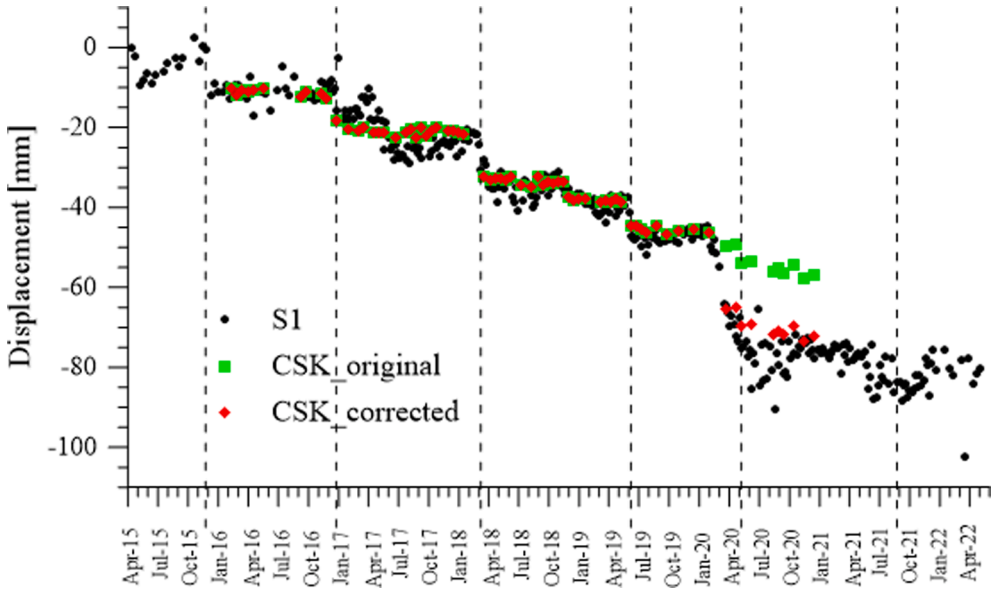

Fig. 11. LoS displacement time series relating to the CSK target G compared to the corresponding time series from S1 (black dots). Green and red dots represent the original and the corrected trend, respectively. (For interpretation of the references to colour in this figure legend, the reader is referred to the web version of this article.)

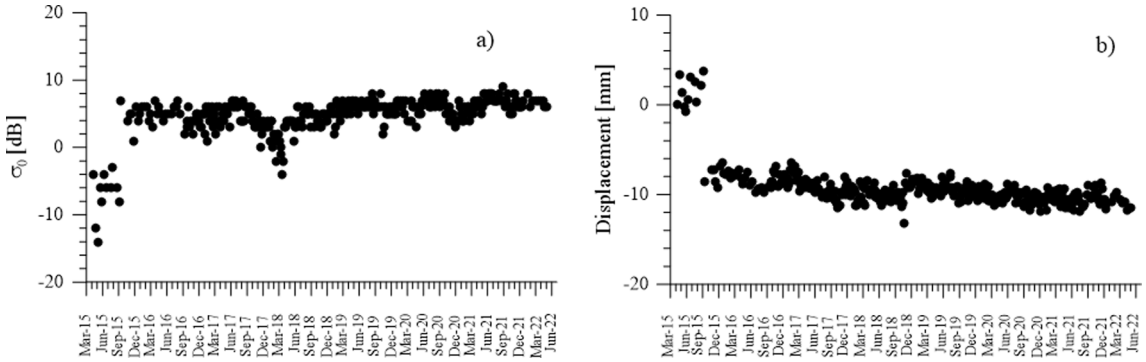

Fig. 12. Effects of a reroofing a) on the backscattering coefficient and b) the corresponding displacement time series.

According to the hypothesis that the displacement field results from the retrogression of failure in the rear scarp of a large landslides, the logged accelerations can be the effect of alternative processes:

1. transient external actions accelerating the failure progression (e.g. water infiltration causing variations of the pore water pressures, or of the suctions in the soil pores);
2. stages of fragile weakening of the soil system underground, prompting more sudden increase of straining (Chandler et al., 1975; Cotecchia & Santaloia, 2021; Potts et al., 1997);
3. local slipping of the soil masses along underground discontinuities, result of the failure progression.

The latter two hypotheses are compatible with a failure progression at the western edge of the slope occurring through the sand and silt strata overlying the higher plasticity and weaker clays, within which failure initiation occurred in the past, and developed largely before involving the stiffer top layers (Cruden and Varnes, 1996). At present, the maximum rates recorded during the recurrent acceleration stage represent a reference for the release of warning thresholds, the exceeding of which is indicative of the possible worsening of the stability conditions.

4.3. *Displacement patterns characterizing the upper part of the slope*

To characterize the displacement patterns over the investigated area, the trend of additional PS, spread out along the range acquisition direction, has been inspected. Reference CSK and corresponding S1 target have been selected along six alignments roughly parallel to the steepest slope path (Fig. 14) using the previous criteria. The main PS parameters are listed in Table 2. The CSK displacement time histories compares fairly well with the S1 displacement data sets, as depicted in Fig. 15 showing the descending displacement of both sensors. No CSK scatterers are present in A3_1 position.

The analysis gives further information about both spatial and temporal features of the displacement field, identifying stable and unstable portions and the timing of the acceleration. Indeed, along the A0 alignment in the southern area a sharp difference in velocity allows to distinguish between stable (A0_2) and unstable (A0_1) zone. Moving northwards, alignments from A1 to A5 are characterized by similar settlement rates. Along both alignments A3 and A4, the points closest to the inner rear scarp, i.e. A3_3 and A4_3 scatterers, show lowest velocities, suggesting a quasi-linear differential trend. Additionally, the analysis performed in azimuth and range directions on both datasets reveals that, in the upper part of the slope, different sectors are location of similar settlement-time trends, which though differ for total displacements, giving further evidence to a spatial distribution of the

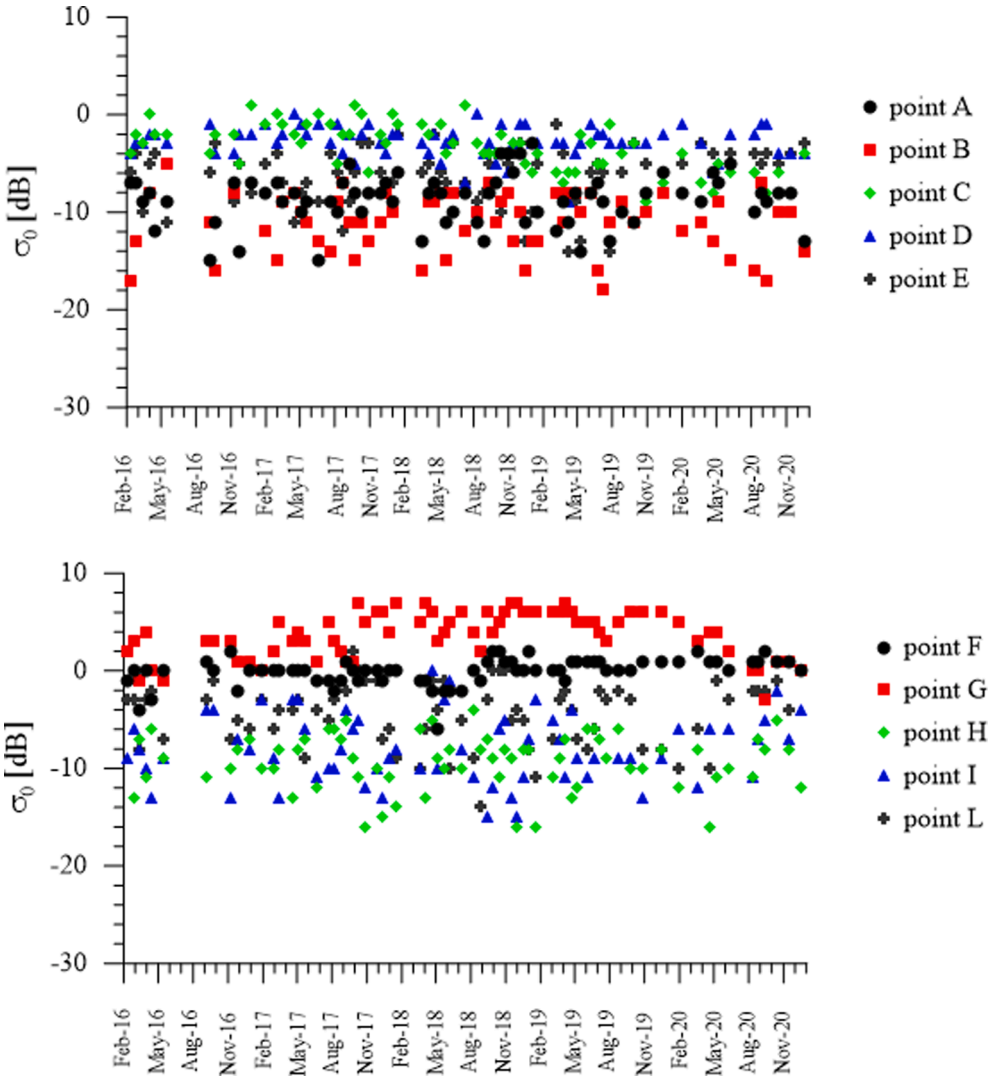

Fig. 13. Backscattering coefficient time evolution of CSK PS located in the unstable area.

displacement rates consistent with a retrogressive attitude of an underground failure.

4.4. Multi-geometry analysis

With the purpose of evaluating horizontal and vertical displacement rates over the longest available timespan, a multi-geometry DInSAR analysis was performed on the S1 dataset, taking advantage from the capability of estimating the mean velocity of a pixel along the east–west and vertical (up-down) tracks by combining ascending and descending datasets (Di Traglia et al., 2021). Both viewing geometries have low sensitivity to north–south displacement, preventing from the detection of the ground motion component along that direction (Pepe & Calò, 2017). However, the investigated slope faces towards west-northwest direction, such that the main component of the planimetric displacement is expected on the east–west direction. Therefore, the east–west (V_E) and up-down (V_U) velocities have been retrieved, adopting a patch approach considering a reduced area within which all selected PS are assumed to be overlapping. This leads to more robust estimations of the 2D components thanks to multiple measurements in the same patch but implies a loss of spatial resolution generated by the observation averaging. After a pre-filtering on the coherence value (≥ 0.7), a 45 m $\times$ 45 m-cell has been identified as the optimal balance between robustness and spatial extent of the investigated phenomenon. The obtained velocity maps gives evidence to a predominant vertical component in the upper portion of the slope, of about −12 mm/year along the area of Via dei Martiri di Via Fani (Fig. 16**b**, light red PS), while low velocities of about −3 mm/year (Fig. 16**a**, yellow PS) are measured in the horizontal direction. The resulting ratio of the vertical to the horizontal velocity of about 4 highlights that the ground block included between the western rear scarp, closest to the retaining wall, and the eastern innermost rear scarp is experiencing mainly vertical movements, suggesting that the most retrogressed portion of the slip surface is sub-vertical. Conversely, the purification plant area is characterized by a predominant horizontal velocity (V_E of about −7 mm/year, Fig. 16**b**, orange dots).

5. Preliminary results of the ground measurements and comparison with MTInSAR outcomes

Following the characterization of the displacement field in the built environment, a ground-based monitoring system (Fig. 17), encompassing 90 levelling benchmarks read once a month using a high-precision digital level, has been established in April 2021. High-resolution biaxial tiltmeters (red triangles in Fig. 17) have been positioned on the retaining wall to check its inclination once per hour.

The levelling measurements, carried out from May 2021 to May 2022, have been used to assess the displacement trends of 8 targets, by comparing them with the observations on levelling benchmarks, i.e. 12,

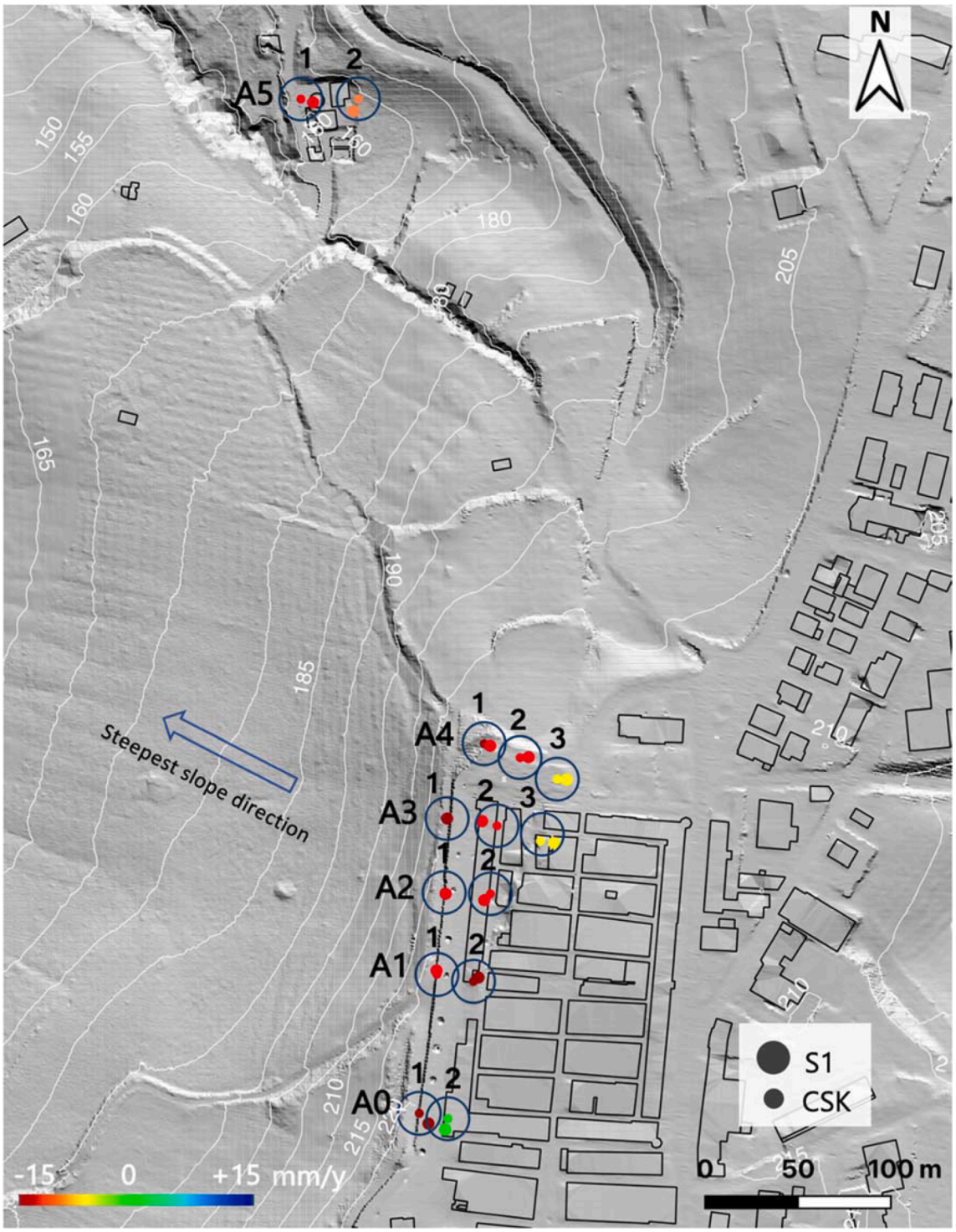

Fig. 14. Analysis of the displacement paths along the LoS. Circles enclose targets selected along the steepest slope. No CSK scatterers are present in A3_1 position (background: LiDAR Digital Elevation Model).

Table 2
Mean coherence and LoS velocity characterizing the PS analyzed along the steepest path.

Satellite	N. of scatterers	Coherence		V Los (mm/year)	
		Mean	St. dev.	Mean	St. dev.
CSK	13	0.7	0.1	−8.4	3
S1	14			−7.8	

17, 20, 25, 29, 65, 66 and 41 in Fig. 17, located in the vicinity of the PS, i.e. A, B, C, E, F, G, H, I in Fig. 8. Since the vertical component of the movement is dominant, and accounting for the limitations discussed in section 4.4, displacements along the LoS and vertical direction are considered comparable (Fig. 10). The ground-based observations confirm the findings achieved through the MTInSAR technique, identifying both the acceleration phase between May and September 2021 and the onset of the transitional period starting from October 2021. The RMSE calculated using the levelling measurements as reference, equal to

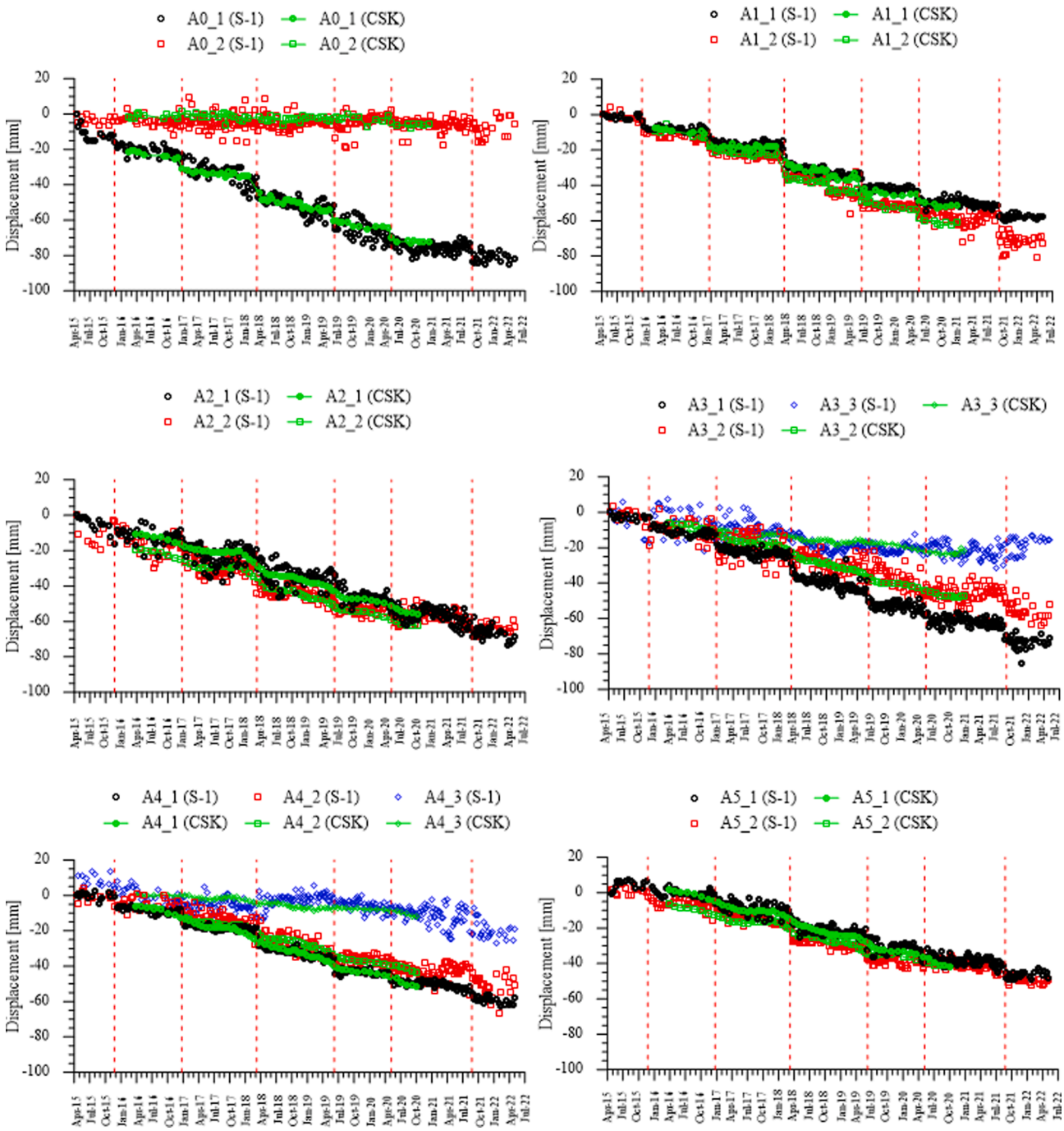

Fig. 15. LoS displacement time series related to fourteen PS (CSK + S1) located along the steepest slope path. Red lines indicate displacement acceleration stages. (For interpretation of the references to colour in this figure legend, the reader is referred to the web version of this article.)

about 2 mm, is below the error on the single displacement measurement (ranging from 2.5 to 4.1 mm for the considered targets) estimated in SPINUA by computing the standard deviation of the differences between the radar displacement measurements and the non-linear model fitting the time series. The inclination $\Delta\theta$ (Fig. 18**a**), measured between September 2021 and May 2022 by the tiltmeters (about $\pm$ 0.02°), shows slight changes with time, mainly related to temperature fluctuations, as observes for the CE04 instrument (Fig. 18). Only the southernmost instrument (CE08), located on a section of the retaining structure affected by a localized failure, recorded increasing values of the inclination, up to 0.1° in March 2022 (Fig. 18**a**). These measurements confirm, once again, the prevalence of the vertical component of the displacement in Via dei Martiri di Via Fani.

6. Evaluation of the possible correlation with the weather conditions

The hypothesis that the non-linear behavior of the system could be related to the climatic actions has been explored through an empirical analysis of the climatic conditions at the site. Slope movements may be connected to climatic conditions affecting the either inward or outward hydraulic fluxes at the ground surface, since these influence the water balance and corresponding piezometric regime across the slope (Guzzetti et al., 2008; Pirone et al., 2012; Tommasi et al., 2013). Generally, shallow ground displacements in fine soil deposits may result from the variation of the pore water pressures over weeks, consequent to the cumulated infiltration of rain-water over 10 to 60 days (cumulative

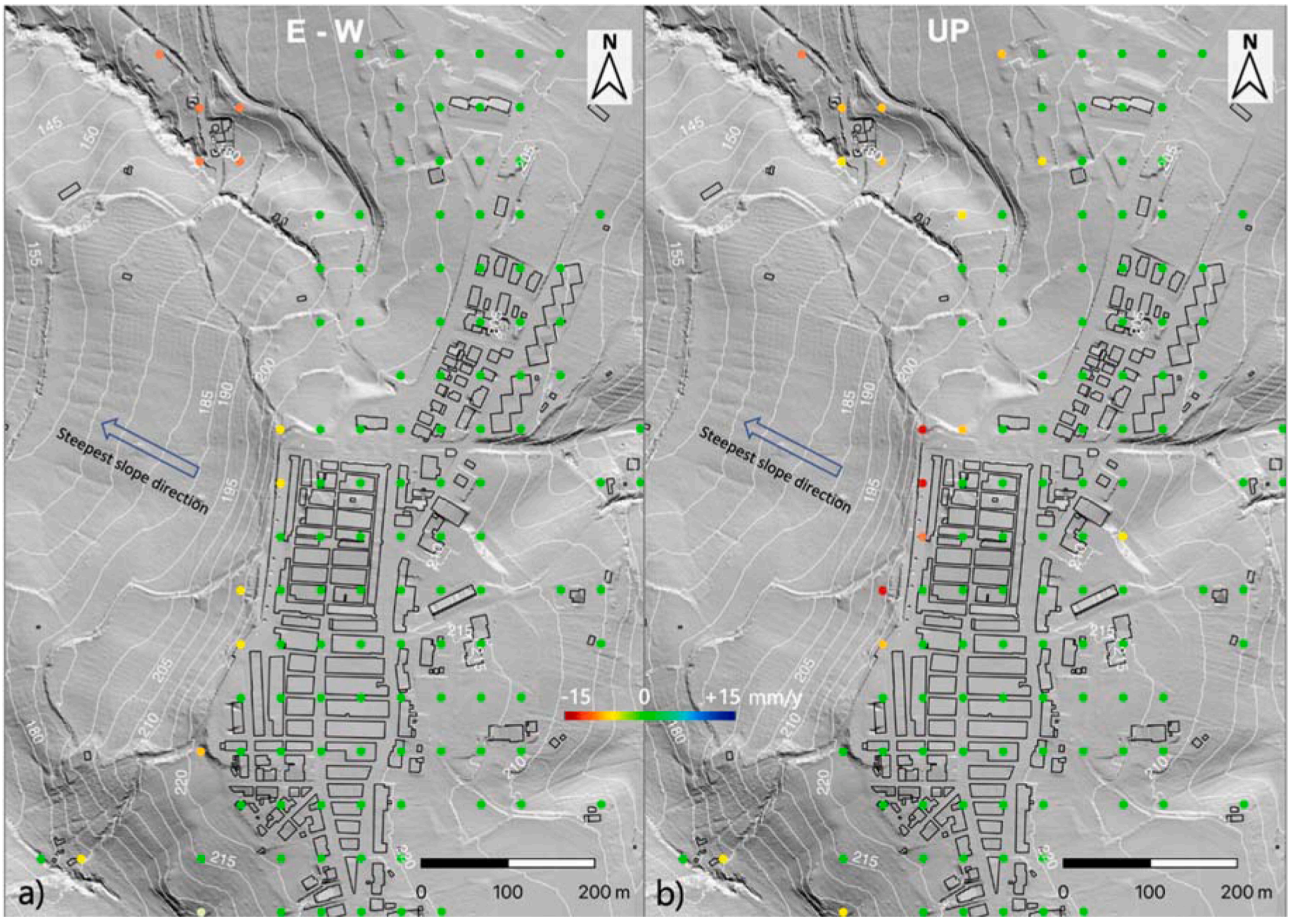

Fig. 16. Displacement rates along the a) east–west and b) up-down directions (background: LiDAR Digital Elevation Model).

rainfalls), where a longer period (90–180 days) might be necessary to trigger deeper slope movements.

Therefore, the possible connection between rainfall infiltration and ground shifts has been evaluated by comparing the cumulative total rainfalls (Ardizzone et al., 2011; Crosta et al., 2017; Hu et al., 2019b) over 30, 60, 90 and 120 days, to the S1 displacement time history of point A (Fig. 8), which undergoes the highest motion along the LoS (Fig. 19**a**). In the same figure, the analysis of the point A displacement gradient, calibrated over a reference period of five SAR image acquisitions approximatively corresponding to the acceleration phase duration, has been performed. The results, presented in Fig. 19**a** with the positive sign, highlight velocity peaks of about 120 mm/year during the acceleration stage, while a quasi-constant velocity might be measured in the transitions between two accelerations, ranging from 7 to 13 mm/year, with an average value of about 10 mm/year. Due to the initial lack of S1 acquisitions, in the period Nov - Dec 2015, the correspondence with peak velocity is not accurately identified, as the revisit time turned into six days only after the introduction of the S1B satellite in September 2016.

Total rainfalls together with the cumulative rainfall time histories, acquired by weather stations of Serracapriola (249 m a.s.l.) and Ripalta (64 m a.s.l), located 5 km and 10 km away from Chieuti town respectively, are depicted in Fig. 19**b and c**. The data between the end of August 2016 and January 2017 were not recorded by Serracapriola station (grey area in Fig. 19**b**). The analysis of both total and cumulative rainfall time histories revealed the same timing, but different amplitude, higher in Serracapriola than in Ripalta, as expected for the altitude of the station.

The comparison of displacement time history with the cumulative rainfalls does not provide a clear indication of any correspondence between the cumulative rainfall peaks, displacement jumps and velocity peaks for either 90 or 120 days of rainfall. A better correlation seems to apply between the peaks of the 30-day cumulative rainfalls and the displacement accelerations, since these occur in correspondence of some 30-day cumulative rainfall peaks, except for the last timespan (Sept–Oct 2021) occurring after a long dry period. However, displacement acceleration does not necessarily concur with 30-day cumulative rainfall peaks. A more refined analysis accounting for the slope-vegetation-atmosphere interaction is foreseen as next step.

7. Discussion and conclusive remarks

C and X-band SAR image stacks, acquired over a period of seven (2015 to 2022) and five years (2015 to 2020) by the S1 and CSK satellite constellations, respectively, has been processed through the SPINUA algorithm. The results enabled the identification of an ongoing instability process affecting the western slope and part of the urban area of the town of Chieuti, whose first evidence dates from the 19th century. The use of multi-sensor SAR data allowed to perform, for the first time regarding this long-standing phenomenon, an accurate definition of the spatial and temporal features of the ground displacement field and the detection of areas characterized by differential displacements inducing damages on structures and infrastructures. An in-depth investigation on a subset of PS, both in range and azimuth direction, brought out non-linear displacement trends with time, where approximately annual periods characterized by relatively slow velocities (10 mm/year on average) are followed by acceleration stages, lasting about one month, during which displacement rate peaks reach about 120 mm/year.

This led to a broader reflection on the actual reliability of MTInSAR techniques in tracking the ground motion for non-linear instability

Fig. 17. Ground-based geomatic system monitoring the urban area (background: LiDAR Digital Elevation Model).

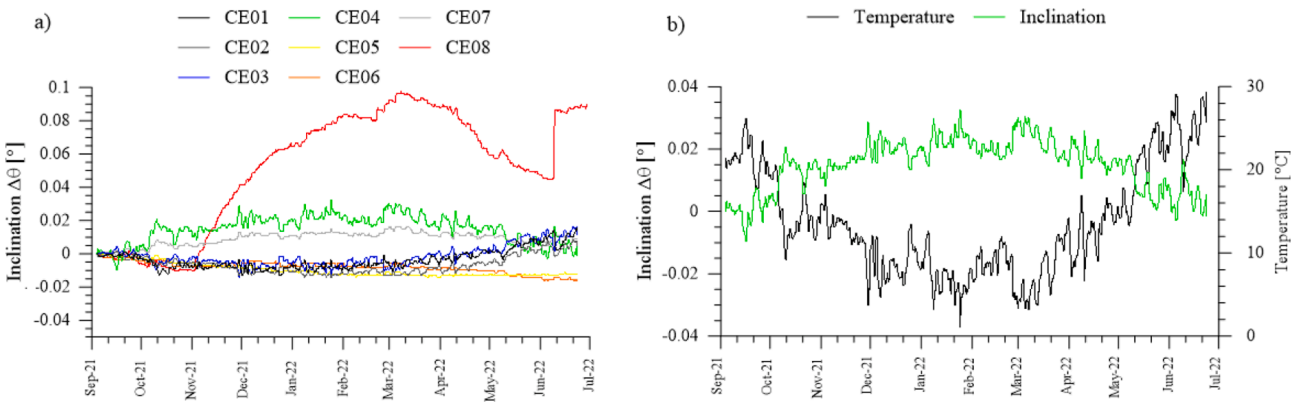

Fig. 18. a) Inclination variations perpendicular to the retaining wall (approximatively along the e-w direction). b) Inclination vs. temperature displayed for the titltmeter CE04.

behaviors. Few studies have addressed this issue, although the analysis of non-linear displacement trends is becoming an increasingly discussed topic. In (Park & Hong, 2021), the a-priori knowledge of the deformation process drove the implementation of a hyperbolic model, adopted to evaluate the non-linear behavior of the three independent subsidence occurrences. Other solutions (Jiang et al., 2021) (Perissin et al., 2012) try to identify non-linearities without having a-priori information on the deformation process. (Chen et al., 2021) compare two well-established techniques (PS and SBAS) by analyzing a S1 dataset on a landslide showing both linear and non-linear behaviors, evidencing the capability of SBAS to better estimate non-linear trends. In (Notti et al., 2014), non-linearities in the landslide kinematics are detected analyzing a Radarsat SAR dataset and focusing on the a-posteriori classification of the time series. A relevant case study regarding a well-known landslide evolving with a non-linear mechanism can be found in (Crosta et al., 2013), where the displacements are monitored through ground-based radar interferometry. In the latter, a similar behavior to the Chieuti landslide is being manifested. However, none of the investigated phenomena highlighted such a well-characterized trend and in no case the employed SAR sensors worked near their ambiguity limit. When displacements show the same order of magnitude of the sensor motion ambiguity limit, as for CSK observations in Chieuti, the processing chain could mistakenly dismiss the corresponding time series, causing a loss of basic information for a proper interpretation of the phenomenon or, contrarywise, producing processing artifacts.

In this study, the integration of multiple SAR datasets allowed to overcome misinterpretations related to the motion ambiguity, also evidencing the reliability of CSK in detecting non-linear displacements in most of the cases, even when working near its resolution. Ground-based measurements, in good agreement with the remote-sensed observations, enhanced the correct interpretation of the retrieved motion patterns. So far, the joint analysis of the available datasets hints a permanent displacement rate trend; however, the monitoring in progress will provide key information on the short-term development of the instability.

The analysis gave evidence to the importance of the open S1 acquisitions, whose time series confirmed the CSK-derived displacement evolution and broaden the period investigated. Therefore, the current reduced availability of S1 data, due to the definitive decommissioning of the S1B satellite announced on 3 August 2022 (ESA, 2022a), might weaken this capability. Whilst the acquisitions carried out by the S1A satellite every twelve days still represent a relevant asset, the full potential of the mission will be reached again with the launch into orbit of the next generation S1C satellite, scheduled in the first half of 2023 (ESA, 2022b).

As regards the characterization of the instability, the MTInSAR analysis allowed to identify the active retrogression of an underground progressive failure within the rear scarp of a large compound roto-translational landslide affecting the western slope, occurring through the sand and silt strata overlying clay layers, location of the failure initiation occurred in the past and recently developing in the stiffer top layers. This retrogressive behavior is confirmed by the evaluation of displacement trends along different alignments, while the multi-geometry analysis and the tiltmeters measurements highlighted the significant prevalence of the vertical component of the instability mechanism in the proximity of the retaining wall, four times higher than the east–west displacement velocity, suggesting that the most retrogressed portion of the slip surface is sub-vertical. Therefore, the research provided indications about the effect of underground failures on the top of the slope connected to the activity of very large soil volumes downslope. The acceleration stages detected through the MTInSAR analysis are indicative of the propagation of these failures, that could be related to weather conditions. Nevertheless, the joint examination of the rainfall data and displacement time histories highlighted a possible, but not clear, correlation. A more reliable assessment of the climatic action influence, currently underway, is taking into account i) the computation of the net rainfall, that is the difference between the total rainfall and the evapotranspiration rates; ii) the numerical computation of the transient seepage through the slope connected to the infiltration of the net rainfall and accounting for the hydraulic and hydrogeological features of the slope, in order to verify the variations with time of the slope stability factor, which might concur with the displacement accelerations.

As this work is framed in a broader project, aimed at further deepening the mechanism generating the ongoing process, the findings presented in this paper are setting the basis for the current studies and will be integrated in a multidisciplinary analysis encompassing surficial and underground data for the three-dimensional modeling of the instability, addressed to the selection of the most sustainable slope stabilization strategy.

Funding

The research has been partially funded by the European Social Fund (ESF) through the National Operational Program Research and Innovation 2014–2020 “Attraction and International Mobility” (PON-AIM project codes AIM1871082-1 and AIM1871082-2, CUP D94I18001600007).

Since 1 September the contribution of F. Cotecchia has been funded through the project PNRR, MISURA M4_C2_1.4 - CAMPIONI NAZIONALI DI R&S - National Centre for HPC, Big Data and Quantum Computing (CN_00000013) - Spoke 5 “Environment and Natural Disasters”.

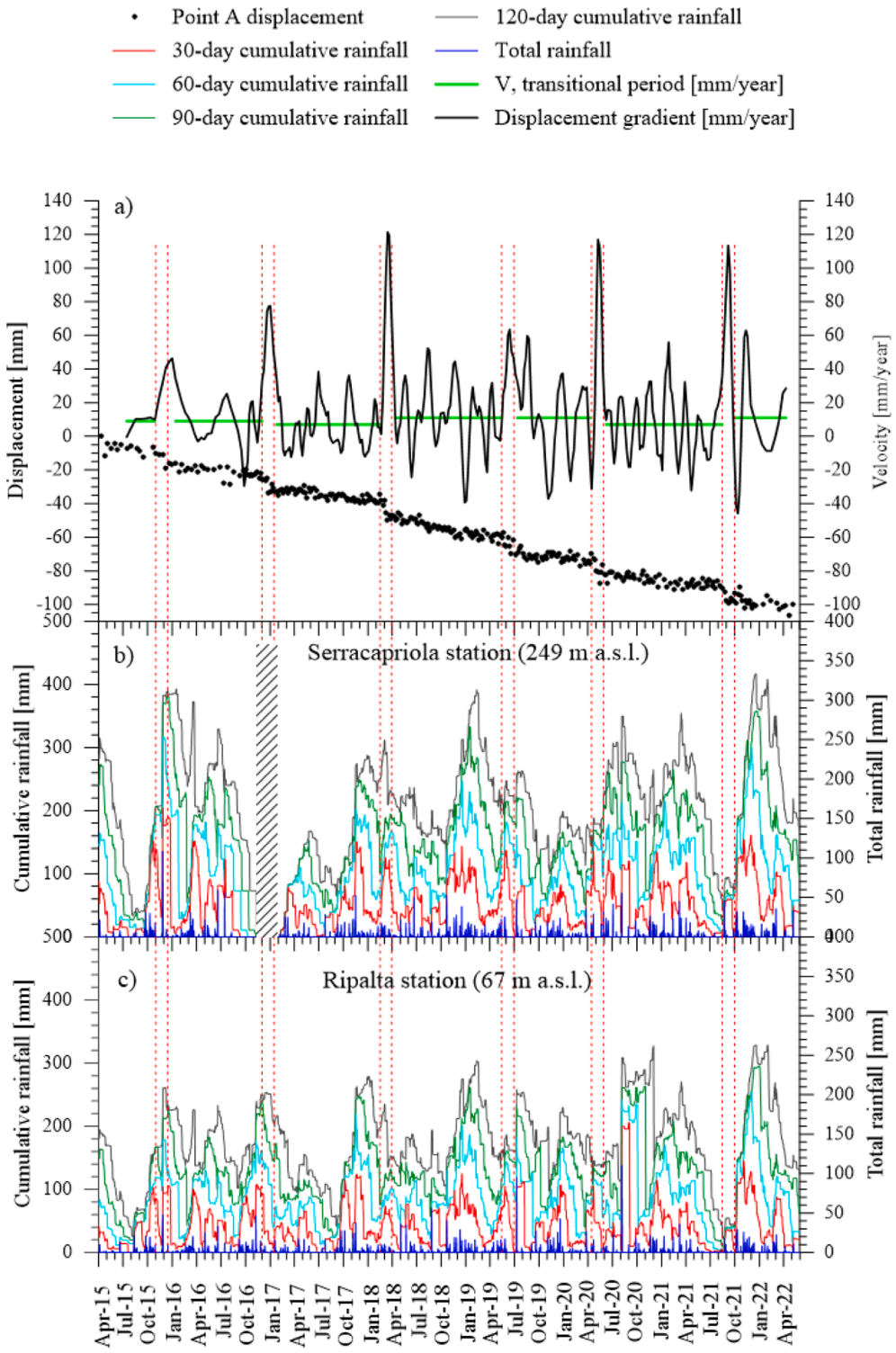

Fig. 19. a) Comparison between point A displacement and the correspondent velocity time history with the cumulative rainfall distributions (30 to 120 days), for dataset acquired by b) Serracapriola and c) Ripalta weather stations.

Declaration of Competing Interest

The authors declare that they have no known competing financial interests or personal relationships that could have appeared to influence the work reported in this paper.

Data availability

The authors do not have permission to share data.

Acknowledgments

This research has been conducted under the agreement between the DICATECh and Government Commissioner for the environmental risk of

Apulia." Authors are grateful to Apogeo and AGLab at Politecnico di Bari for their support in the levelling measurements and Planetek Italia for making available the MTInSAR dataset. All authors have read and agreed to the published version of the manuscript.

References

Achu, A.L., Joseph, S., Aju, C.D., Mathai, J., 2021. Preliminary analysis of a catastrophic landslide event on 6 August 2020 at Pettimudi, Kerala State, India. Landslides 18 (4). https://doi.org/10.1007/s10346-020-01598-x.

Alonso, E. E., Pinyol, N. M., & Puzrin, A. M. (2010). Catastrophic Slide: Vaiont Landslide, Italy. In *Geomechanics of Failures. Advanced Topics*. https://doi.org/10.1007/978-90-481-3538-7_2.

Ardizzone, F., Rossi, M., Calò, F., Paglia, L., Manunta, M., Mondini, A.C., Zeni, G., Reichenbach, P., Lanari, R., Guzzetti, F., 2011. Preliminary analysis of a correlation between ground deformations and rainfall: the Ivancich landslide, central Italy. SAR Image Analysis, Modeling, and Techniques XI 8179. https://doi.org/10.1117/12.899453.

Artese, S., Perrelli, M., 2018. Monitoring a landslide with high accuracy by total station: A DTM-based model to correct for the atmospheric effects. Geosciences (Switzerland) 8 (2). https://doi.org/10.3390/geosciences8020046.

Barat, I., Prats, P., Duesmann, B., & Geudtner, D. (2015). Sentinel-1: Link Between Orbit Control and Interferometric Sar Baselines Performance. *25th International Symposium on Space Flight Dynamics ISSFD*, *1*.

Bitelli, G., Roncari, G., Tini, M.A., Vittuari, L., 2018. High-precision topographical methodology for determining height differences when crossing impassable areas. Measur.: J. Int. Measur. Conf. 118 https://doi.org/10.1016/j.measurement.2018.01.013.

Bovenga, F., Nitti, D.O., Fornaro, G., Radicioni, F., Stoppini, A., Brigante, R., 2013. Using C/X-band SAR interferometry and GNSS measurements for the Assisi landslide analysis. Int. J. Remote Sens. 34 (11) https://doi.org/10.1080/01431161.2013.772310.

Bovenga, F., Nutricato, R., Refice, A., Guerriero, L., & Chiaradia, M. T. (2005). SPINUA: A flexible processing chain for ERS / ENVISAT long term interferometry. *European Space Agency, (Special Publication) ESA SP*, *572*.

Calò, F., Ardizzone, F., Castaldo, R., Lollino, P., Tizzani, P., Guzzetti, F., Lanari, R., Angeli, M.G., Pontoni, F., Manunta, M., 2014. Enhanced landslide investigations through advanced DInSAR techniques: The Ivancich case study, Assisi, Italy. *Rem. Sens. Environ.* 142 https://doi.org/10.1016/j.rse.2013.11.003.

Chandler, R.J., Skempton, A.W., Muir Wood, A.M., 1975. The Design of Permanent Cutting Slopes in Stiff Fissured Clays. Geotechnique 25 (2). https://doi.org/10.1680/geot.1975.25.2.425.

Chen, X., Tessari, G., Fabris, M., Achilli, V., & Floris, M. (2021). *Comparison Between PS and SBAS InSAR Techniques in Monitoring Shallow Landslides*. https://doi.org/10.1007/978-3-030-60311-3_17.

Cotecchia, F., & Santaloia, F. (2021). *Mitigazione del Rischio da Frana per lo Sviluppo Sostenibile e la Tutela dell'Ambiente. General Report per il XXVII Convegno Nazionale di Geotecnica. Università degli Studi "Mediterranea" Reggio Calabria, 7 – 9 luglio 2021*.

Cotecchia, F., Santaloia, F., Tagarelli, V., 2020. Towards A Geo-Hydro-Mechanical Characterization of Landslide Classes: Preliminary Results. Appl. Sci. 10 (22), 7960. https://doi.org/10.3390/app10227960.

Crespi, M., Giannone, F., Marsella, M., & Sonnessa, A. (2012). Automated geomatic system for monitoring historical buildings during tunneling in Roma, Italy. *Life-Cycle and Sustainability of Civil Infrastructure Systems - Proceedings of the 3rd International Symposium on Life-Cycle Civil Engineering, IALCCE 2012*.

Crosetto, M., Monserrat, O., Cuevas-González, M., Devanthéry, N., & Crippa, B. (2016). Persistent Scatterer Interferometry: A review. In *ISPRS Journal of Photogrammetry and Remote Sensing* (Vol. 115). https://doi.org/10.1016/j.isprsjprs.2015.10.011.

Crosta, G.B., Agliardi, F., Rivolta, C., Alberti, S., Dei Cas, L., 2017. Long-term evolution and early warning strategies for complex rockslides by real-time monitoring. Landslides 14 (5). https://doi.org/10.1007/s10346-017-0817-8.

Crosta, G.B., di Prisco, C., Frattini, P., Frigerio, G., Castellanza, R., Agliardi, F., 2013. Chasing a complete understanding of the triggering mechanisms of a large rapidly evolving rockslide. Landslides 11 (5). https://doi.org/10.1007/s10346-013-0433-1.

Cruden, D.M., Varnes, D.J., 1996. Landslide types and processes. Special Report - National Research Council, Transportation Research Board, p. 247.

Dai, F.C., Lee, C.F., Ngai, Y.Y., 2002. Landslide risk assessment and management: An overview. Eng. Geol. 64 (1) https://doi.org/10.1016/S0013-7952(01)00093-X.

de Luna, R.M.R., dos Anjos Garnés, S.J., da Silva Pereira Cabral, J.J., dos Santos, S.M., 2017. Groundwater overexploitation and soil subsidence monitoring on Recife plain (Brazil). Nat Hazards 86 (3). https://doi.org/10.1007/s11069-017-2749-y.

Del Soldato, M., Farolfi, G., Rosi, A., Raspini, F., Casagli, N., 2018. Subsidence evolution of the Firenze-Prato-Pistoia plain (Central Italy) combining PSI and GNSS data. Remote Sens. (Basel) 10 (7). https://doi.org/10.3390/rs10071146.

Di Traglia, F., De Luca, C., Manzo, M., Nolesini, T., Casagli, N., Lanari, R., Casu, F., 2021. Joint exploitation of space-borne and ground-based multitemporal InSAR measurements for volcano monitoring: The Stromboli volcano case study. Remote Sens. Environ. 260 https://doi.org/10.1016/j.rse.2021.112441.

ESA. (2022a). *Mission ends for Copernicus Sentinel-1B satellite*.

ESA. (2022b). *Ride into orbit secured for Sentinel-1C*.

Esposito, G., Carabella, C., Paglia, G., Miccadei, E., 2021. Relationships between morphostructural/geological framework and landslide types: Historical landslides in the hilly piedmont area of abruzzo region (central Italy). Land 10 (3). https://doi.org/10.3390/land10030287.

Even, M., Schulz, K., 2018. InSAR deformation analysis with distributed scatterers: A review complemented by new advances. Remote Sens. 10 (5) https://doi.org/10.3390/rs10050744.

Ferretti, A., Prati, C., Rocca, F., 2001. Permanent scatterers in SAR interferometry. IEEE Trans. Geosci. Remote Sens. 39 (1) https://doi.org/10.1109/36.898661.

Furst, S.L., Doucet, S., Vernant, P., Champollion, C., Carme, J.L., 2021. Monitoring surface deformation of deep salt mining in Vauvert (France), combining InSAR and leveling data for multi-source inversion. *Solid.* Earth 12 (1). https://doi.org/10.5194/se-12-15-2021.

Guzzetti, F., Peruccacci, S., Rossi, M., Stark, C.P., 2008. The rainfall intensity-duration control of shallow landslides and debris flows: An update. Landslides 5 (1), 3–17. https://doi.org/10.1007/S10346-007-0112-1/FIGURES/8.

Hsu, Y.J., Lai, Y.R., You, R.J., Chen, H.Y., Teng, L.S., Tsai, Y.C., Tang, C.H., Su, H.H., 2018. Detecting rock uplift across southern Taiwan mountain belt by integrated GPS and leveling data. Tectonophysics 744. https://doi.org/10.1016/j.tecto.2018.07.012.

Hu, F., van Leijen, F.J., Chang, L., Wu, J., Hanssen, R.F., 2019a. Monitoring deformation along railway systems combining Multi-temporal InSAR and LiDAR data. Remote Sens. (Basel) 11 (19). https://doi.org/10.3390/rs11192298.

Hu, X., Bürgmann, R., Lu, Z., Handwerger, A.L., Wang, T., Miao, R., 2019b. Mobility, Thickness, and Hydraulic Diffusivity of the Slow-Moving Monroe Landslide in California Revealed by L-Band Satellite Radar Interferometry. *Journal of Geophysical Research: Solid*. Earth 124 (7). https://doi.org/10.1029/2019JB017560.

Hungr, O., Leroueil, S., Picarelli, L., 2014. The Varnes classification of landslide types, an update. Landslides 11, 167–194. https://doi.org/10.1007/s10346-013-0436-y.

Jiang, H., Balz, T., Cigna, F., Tapete, D., 2021. Land subsidence in wuhan revealed using a non-linear PSInSAR approach with long time series of COSMO-SkyMed SAR data. Remote Sens. (Basel) 13 (7). https://doi.org/10.3390/rs13071256.

Karila, K., Karjalainen, M., Hyyppä, J., Koskinen, J., Saaranen, V., Rouhiainen, P., 2013. A comparison of precise leveling and Persistent Scatterer SAR Interferometry for building subsidence rate measurement. ISPRS Int. J. Geo Inf. 2 (3) https://doi.org/10.3390/ijgi2030797.

Mazzanti, P., Bozzano, F., Cipriani, I., Prestininzi, A., 2015. New insights into the temporal prediction of landslides by a terrestrial SAR interferometry monitoring case study. Landslides 12 (1). https://doi.org/10.1007/s10346-014-0469-x.

Milillo, P., Riel, B., Minchew, B., Yun, S.H., Simons, M., Lundgren, P., 2016. On the Synergistic Use of SAR Constellations' Data Exploitation for Earth Science and Natural Hazard Response. IEEE J. Sel. Top. Appl. Earth Obs. Remote Sens. 9 (3) https://doi.org/10.1109/JSTARS.2015.2465166.

Morgese, M., Ansari, F., Domaneschi, M., Cimellaro, G.P., 2020. Post-collapse analysis of Morandi's Polcevera viaduct in Genoa Italy. *Journal of Civil*. Struct. Health Monit. 10 (1) https://doi.org/10.1007/s13349-019-00370-7.

Nibigira, L., Havenith, H.B., Archambeau, P., Dewals, B., 2018. Formation, breaching and flood consequences of a landslide dam near Bujumbura, Burundi. Nat. Hazards Earth Syst. Sci. 18 (7) https://doi.org/10.5194/nhess-18-1867-2018.

Nitti, D.O., Hanssen, R.F., Refice, A., Bovenga, F., Nutricato, R., 2011. Impact of DEM-assisted coregistration on high-resolution SAR interferometry. IEEE Trans. Geosci. Remote Sens. 49 (3) https://doi.org/10.1109/TGRS.2010.2074204.

Notti, D., Meisina, C., Zucca, F., Colombo, A., 2014. Non linear PS time series: Analysis and post-processing for landslides studies. Lecture Notes in Earth Syst. Sci. https://doi.org/10.1007/978-3-642-32408-6_56.

Park, S.W., Hong, S.H., 2021. Nonlinear Modeling of Subsidence From a Decade of InSAR Time Series. Geophys. Res. Lett. 48 (3) https://doi.org/10.1029/2020GL090970.

Pepe, A., Calò, F., 2017. A review of interferometric synthetic aperture RADAR (InSAR) multi-track approaches for the retrieval of Earth's Surface displacements. Appl. Sci. (Switzerland) 7 (12). https://doi.org/10.3390/app7121264.

Perissin, D., Wang, Z., Lin, H., 2012. Shanghai subway tunnels and highways monitoring through Cosmo-SkyMed Persistent Scatterers. ISPRS J. Photogramm. Remote Sens. 73 https://doi.org/10.1016/j.isprsjprs.2012.07.002.

Pirone, M., Damiano, E., Picarelli, L., Olivares, L., Urciuoli, G., 2012. Groundwater-atmosphere interaction in unsaturated pyroclastic slopes at two sites in Italy. Italian Geotech. J. 66 (3), 29–49.

Potts, D.M., Kovacevlc, N., Vaughan, P.R., 1997. Delayed collapse of cut slopes in stiff clay. Geotechnique 47 (5). https://doi.org/10.1680/geot.1997.47.5.953.

Prats-Iraola, P., Scheiber, R., Marotti, L., Wollstadt, S., Reigber, A., 2012. TOPS interferometry with terraSAR-X. IEEE Trans. Geosci. Remote Sens. 50 (8) https://doi.org/10.1109/TGRS.2011.2178247.

Radicioni, F., Stoppini, A., Brigante, R., Fornaro, G., Bovenga, F., & Nitti, D. O. (2012). Long-term GNSS and SAR data comparison for the deformation monitoring of the Assisi landslide. *FIG Working Week 2012*.

Raspini, F., Bardi, F., Bianchini, S., Ciampalini, A., Del Ventisette, C., Farina, P., Ferrigno, F., Solari, L., Casagli, N., 2017. The contribution of satellite SAR-derived displacement measurements in landslide risk management practices. Nat. Hazards 86 (1). https://doi.org/10.1007/s11069-016-2691-4.

Raspini, F., Bianchini, S., Ciampalini, A., Del Soldato, M., Solari, L., Novali, F., Del Conte, S., Rucci, A., Ferretti, A., Casagli, N., 2018. Continuous, semi-automatic monitoring of ground deformation using Sentinel-1 satellites. Sci. Rep. 8 (1) https://doi.org/10.1038/s41598-018-25369-w.

Reale, D., Nitti, D.O., Peduto, D., Nutricato, R., Bovenga, F., Fornaro, G., 2011. Postseismic deformation monitoring with the COSMO/SKYMED constellation. IEEE Geosci. Remote Sens. Lett. 8 (4) https://doi.org/10.1109/LGRS.2010.2100364.

Schubert, A., Small, D., Miranda, N., Geudtner, D., Meier, E., 2015. Sentinel-1A product geolocation accuracy: Commissioning phase results. Remote Sens. (Basel) 7 (7). https://doi.org/10.3390/rs70709431.

Scifoni, S., Bonano, M., Marsella, M., Sonnessa, A., Tagliafierro, V., Manunta, M., Lanari, R., Ojha, C., Sciotti, M., 2016. On the joint exploitation of long-term DInSAR

time series and geological information for the investigation of ground settlements in the town of Roma (Italy). Remote Sens. Environ. 182 https://doi.org/10.1016/j.rse.2016.04.017.

Shi, X., Zhang, L., Zhong, Y., Zhang, L., Liao, M., 2020. Detection and characterization of active slope deformations with Sentinel-1 InSAR analyses in the southwest area of Shanxi, China. Remote Sens. (Basel) 12 (3). https://doi.org/10.3390/rs12030392.

Sonnessa, A., Cantatore, E., Esposito, D., & Fiorito, F. (2020). A Multidisciplinary Approach for Multi-risk Analysis and Monitoring of Influence of SODs and RODs on Historic Centres: The ResCUDE Project. *Lecture Notes in Computer Science (Including Subseries Lecture Notes in Artificial Intelligence and Lecture Notes in Bioinformatics)*, *12252 LNCS*. https://doi.org/10.1007/978-3-030-58811-3_54.

Sonnessa, A., & Tarantino, E. (2021). *Using GNSS Observation for Mitigating the Impact of SODs and RODs on the Built Environment – Introducing the New SNIK Continuously Operating Reference Station and Its Applications*. https://doi.org/10.1007/978-3-030-87007-2_8.

Tommasi, P., Boldini, D., Caldarini, G., Coli, N., 2013. Influence of infiltration on the periodic re-activation of slow movements in an overconsolidated clay slope. Can. Geotech. J. 50 (1), 54–67. https://doi.org/10.1139/cgj-2012-0121.

Uemoto, J., Moriyama, T., Nadai, A., Kojima, S., Umehara, T., 2019. Landslide detection based on height and amplitude differences using pre- and post-event airborne X-band SAR data. Nat. Hazards 95 (3). https://doi.org/10.1007/s11069-018-3492-8.

Vaníček, P., Craymer, M.R., Krakiwsky, E.J., 2001. Robustness analysis of geodetic horizontal networks. J. Geod. 75 (4) https://doi.org/10.1007/s001900100162.

Wasowski, J., Bovenga, F., 2015. Remote Sensing of Landslide Motion with Emphasis on Satellite Multitemporal Interferometry Applications: An Overview. In *Landslide Hazards, Risks, and Disasters*. https://doi.org/10.1016/B978-0-12-396452-6.00011-2.